Article

Schwann Cells in the Ventral Dermis Do Not Derive from Myf5-Expressing Precursors

Haizea Iribar,[1] Virginia Pérez-López,[1] Usue Etxaniz,[1] Araika Gutiérrez-Rivera,[1,*] and Ander Izeta[1,2,*]
[1]Tissue Engineering Laboratory, Bioengineering Area, Instituto Biodonostia, San Sebastian 20014, Spain
[2]Department of Biomedical Engineering, School of Engineering, Tecnun-University of Navarra, San Sebastian 20009, Spain
*Correspondence: araika.gutierrez@biodonostia.org (A.G.-R.), ander.izeta@biodonostia.org (A.I.)
https://doi.org/10.1016/j.stemcr.2017.09.010

SUMMARY

The embryonic origin of lineage precursors of the trunk dermis is somewhat controversial. Precursor cells traced by *Myf5* and *Twist2* (*Dermo1*) promoter activation (i.e., cells of presumed dermomyotomal lineage) have been reported to generate Schwann cells. On the other hand, abundant data demonstrate that dermal Schwann cells derive from the neural crest. This is relevant because dermal precursors give rise to neural lineages, and multilineage differentiation potential qualifies them as adult stem cells. However, it is currently unclear whether neural lineages arise from dedifferentiated Schwann cells instead of mesodermally derived dermal precursor cells. To clarify these discrepancies, we traced SOX2+ adult dermal precursor cells by two independent *Myf5* lineage tracing strains. We demonstrate that dermal Schwann cells do not belong to the *Myf5+* cell lineage, indicating that previous tracing data reflected aberrant *cre* recombinase expression and that bona fide *Myf5+* dermal precursors cannot transdifferentiate to neural lineages in physiological conditions.

INTRODUCTION

The developmental origin of adult stem cells affects their differentiation potential. Thus, a proper understanding of cell lineage specification may be considered as a prerequisite for safe and efficacious use in the clinic. Adult skin-derived precursors might represent a useful tool for novel cell-based therapies (Agabalyan et al., 2017; Hunt et al., 2009), and their use in the potential treatment of neurodegenerative disease has long been pursued (Joannides et al., 2004). However, the developmental origins and relationships of the diverse adult stem cell pools in the dermis are poorly understood (Dupin and Sommer, 2012). The classical view is that craniofacial dermis originates in the neural crest. In accordance, the dermal precursors in this region are neural crest-derived and thus traced by the *Wnt1-cre* construct (Fernandes et al., 2004). In the trunk dermis, dorsal precursors present a somitic origin while ventrolateral precursors derive from the lateral plate mesoderm (Christ et al., 2007; Millar, 2005; Olivera-Martinez et al., 2004). Consistent with embryonic development, adult dorsal but not ventral trunk precursors are traced by the *Myf5-cre[Sor]* construct (Jinno et al., 2010). The fact that dorsal mesoderm-derived (*Dermo1-cre+*) precursors efficiently give rise to functional Schwann cells, both *in vitro* and in cell transplants (Krause et al., 2014), is puzzling for a number of reasons. First, Schwann cells originate in the neural crest (Jessen et al., 2015) and there is no known evidence of physiological mesenchymal-to-Schwann cell transitions in development. Second, dorsal precursors with the capacity to generate neural crest derivatives seem to represent terminal Schwann cells and melanocytes resident in the mouse skin, both cell types being neural crest-derived

(Gresset et al., 2015). Third, the endogenous dorsal precursors implicated in the dermal response to wounding are also neural crest-derived (Johnston et al., 2013; Krause et al., 2014). Finally, SOX2+ dermal precursor cells of human foreskin belong to the Schwann and perivascular lineages (Etxaniz et al., 2014), which again seem consistent with a neural crest origin.

It is currently unknown whether the dermal precursors that operate in development are identical to those relevant in adult dermal homeostasis and in the dermal response to injury (Agabalyan et al., 2016). To shed light on the relationship between embryonic and adult precursors and to facilitate translation to the clinic of adult human dermal precursor cells, in this work we aimed to identify the origin of adult ventral precursors by lineage tracing experiments in the mouse dermis. We demonstrate that the tracing by *Myf5-cre[Sor]* mice does not actually represent the existence of a mesodermally derived cell population that generates Schwann cells (Jinno et al., 2010; Krause et al., 2014), thus suggesting that the neural progeny of dermal stem cell cultures derives from widespread neural crest precursors, most possibly the Schwann cells ensheathing peripheral nerves.

RESULTS

A SOX2+ Cell Population Traced by *Myf5-cre[Sor]* Expression Retains Neural Competence in Ventral Trunk Dermis

To trace the lineage of precursor cells in the dorsal and ventral dermis, we chose the same transgenic mouse line that had been previously used to express *cre* recombinase under the control of the *Myf5* promoter (*Myf5-cre[Sor]*)
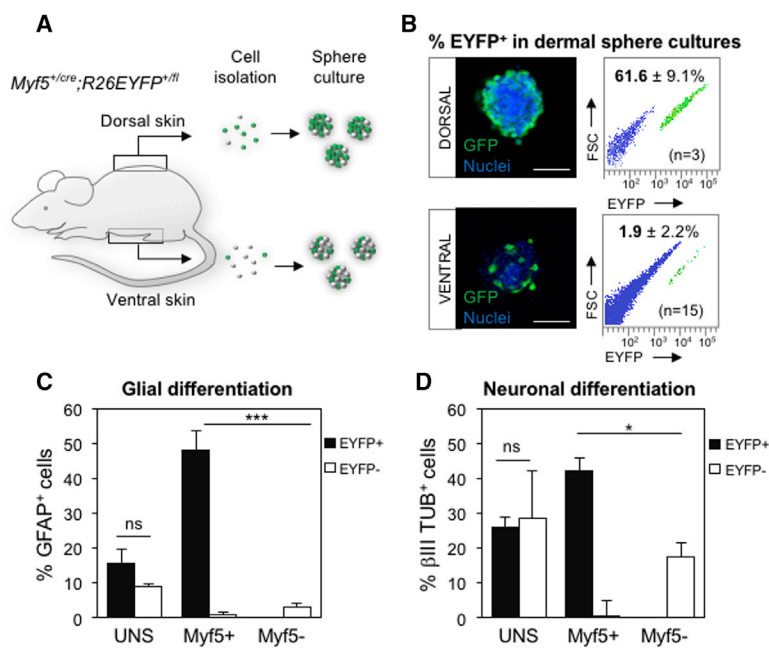
Figure 1. A *Myf5*^{+} Neural-Competent Cell Population in Mouse Ventral Dermis

(A) Scheme of the isolation and culture of dermal precursors from *Myf5*[+/cre]*;R26EYFP*^{+/fl} mouse skin.

(B) Characterization of primary dermal spheres by immunofluorescence (IF) and flow cytometry. Left panels (IF): EYFP expression was detected with anti-GFP antibody (green) and cell nuclei were counterstained with Hoechst 33258 (blue). Scale bars, 50 μm. Right panels (flow cytometry): *Myf5*^{+} cell percentages (mean ± SD) were determined by EYFP expression in sphere cultures (n, number of independent biological replicates).

(C and D) *In vitro* neural differentiation of unsorted (UNS), *Myf5*^{+}, and *Myf5*^{−} cell fractions isolated by FACS from *Myf5*[cre/+]*;R26*[EYFP] ventral dermal spheres. Quantification of the neural progeny as percentage of GFAP^{+} cells (C) and βIII TUBULIN^{+} cells (D) in UNS, *Myf5*^{+}, and *Myf5*^{−} cell fractions in relation to the total number of cells are shown. Bars represent means ± SEM. Statistical significance values (determined by two-tailed unpaired t test) were: in (C), p = 0.1975 (not significant; ns) for the comparison of EYFP[+] versus EYFP[−] in UNS condition and ***p = 0.0004 for the comparison of EYFP[+] (*Myf5*^{+}) versus EYFP[−] (*Myf5*^{−}) fractions; in (D), p = 0.771 (ns) for the comparison of EYFP[+] versus EYFP[−] populations in the UNS fraction and *p = 0.01 for the comparison of EYFP+ (*Myf5*^{+}) versus EYFP[−] (*Myf5*^{−}) fractions. See also Figures S1 and S2.

(Jinno et al., 2010), and crossed it with R26EYFP^{+/fl} reporter mice (Figure 1). Dorsal and ventral dermis-derived precursors from *Myf5*[cre/+]*;R26*[EYFP] double transgenic mice were isolated and expanded in sphere culture (Figure 1A). Consistent with previous reports, a majority (61.6% ± 9.1%, n = 3) of sphere cells from back skin were traced by *Myf5-cre*[Sor] expression (EYFP^{+} cells), as assessed by immunofluorescence and flow cytometry (Figure 1B). In the ventral dermis, we noticed the existence of a small and previously overlooked *Myf5*^{+} cell population (1.9% ± 2.2%, n = 15) that was difficult to reconcile with a lateral plate mesoderm origin of precursor cells in this region (Ohtola et al., 2008). Besides a morphology consistent with neural-competent, dedifferentiated Schwann cells (lower panel of Figure 1B; see also Figure S1 and Etxaniz et al., 2014), the *Myf5*^{+} cells expressed neural precursor cell marker NESTIN (Figure S1). To determine whether the *Myf5*^{+} cells from ventral skin presented *in vitro* neural differentiation capacities, we isolated cell fractions from *Myf5*[cre/+]*;R26*[EYFP] mice by fluorescence-activated cell sorting (FACS) through EYFP expression, put them into differentiation media, and quantified their neural progeny by immunofluorescence with anti-GFAP and anti-βIII TUBULIN antibodies (Figures 1C and 1D). In both cases, the *Myf5*^{+} cells showed a significant increase in neural differentiation capacity when compared with the *Myf5*^{−} fraction, which was more evident for the glial-specific antibody GFAP (15.5-fold versus 2.5-fold increase in βIII TUBULIN^{+} cells; Figures 1C and

1D). Furthermore, the differentiated cultures of the *Myf5*^{+} fraction presented a characteristic bipolar glial morphology that was corroborated by co-staining with markers p75NTR, GFAP, βIII TUBULIN, and S100β (Figures S1A–S1P). Interestingly, *Myf5*^{+} cells expressed SOX2, a transcription factor associated with dermal stem cells (Figures S1Q–S1T'). These data suggested that a SOX2^{+} neural precursor cell population (unexpectedly traced by *Myf5* expression) retained neural competence in mouse ventral dermis.

To further characterize *in vitro* differentiated cells, we determined the expression of key markers of the Schwann cell lineage (Etxaniz et al., 2014) by real-time qRT-PCR (Figure S2). We selected the genes *Ngfr* (coding for p75NTR), *Cdh19* (CADHERIN 19), *Egr1* (KROX24), *Gap43* (GAP43), *Ncam1* (CD56), *S100b* (S100β), and *Egr2* (KROX20) to discriminate between the different stages of Schwann cell lineage determination (Figures S2A and S2B). Analysis of mRNA expression for these genes demonstrated that markers specific of Schwann cell precursors (SCP), such as *Cdh19*, as well as genes shared by SCPs and immature Schwann cells (such as *Egr1* and *Gap43*) were upregulated in differentiated *Myf5*^{+} cells, indicating that significant numbers of cells remained in precursor state in culture. The more differentiated cells seem to belong to the non-myelinating Schwann lineage as shown by the expression patterns of *Ngfr*, *Gap43*, *Ncam1*, *S100b*, and *Egr2* (Figure S2C). In all, these data suggested that *Myf5-cre*[Sor+] cells might belong to the Schwann lineage and give rise to Schwann cells *in vitro*.
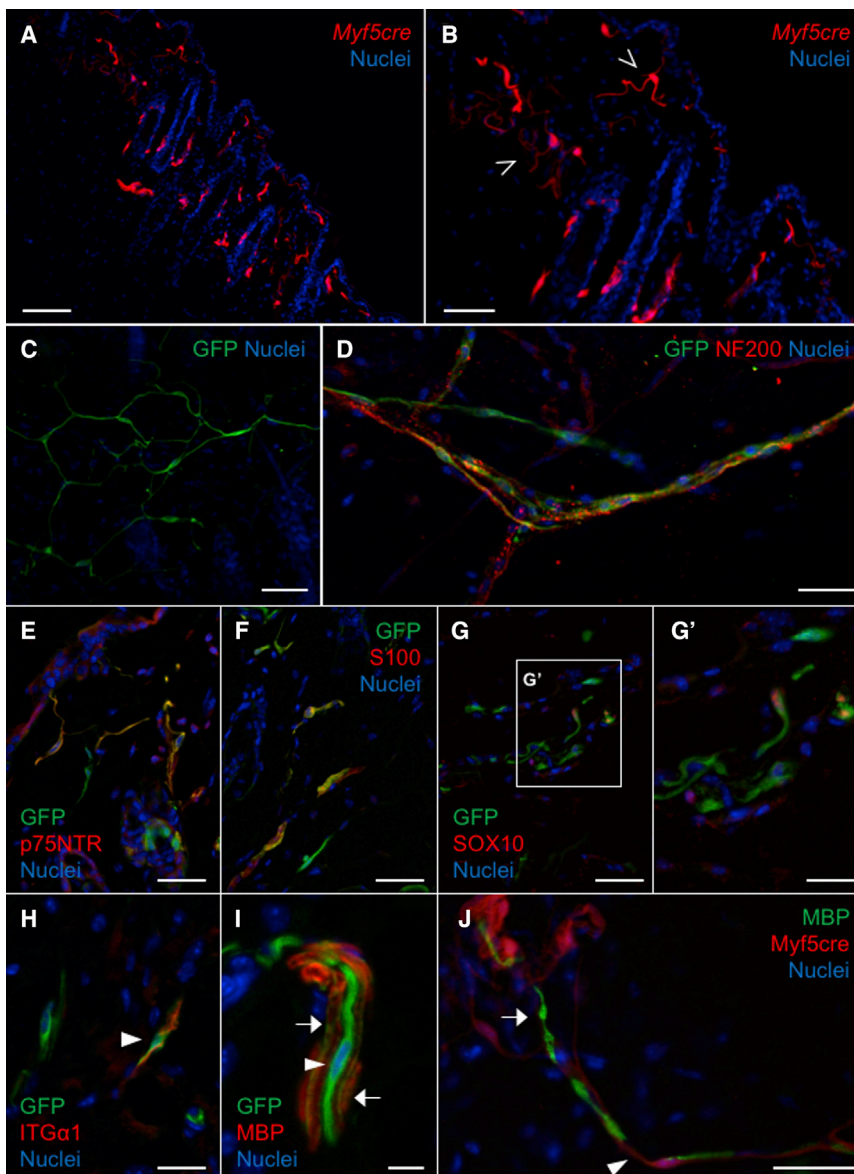
Figure 2. *In Situ* Localization of *Myf5*+ Cells in Mouse Ventral Dermis

(A and B) Ventral skin sections of *Myf5cre/+;R26TdTomato* were directly visualized under the microscope and showed a nerve fiber-like pattern of *Myf5* expression (TdTomato, red) across the entire dermal papillary layer. Open arrowheads in (B) point to Schwann cells (SC) of the subepidermal plexus.

(C and D) Whole-mount preparations of *Myf5cre/+;R26EYFP* ventral dermis were stained with anti-GFP (to detect EYFP, green) and imaged in (C) at the subepidermal plexus level and in (D) in thin subepidermal nerves running along NF200+ (red) peripheral axons.

(E–G') *Myf5*+ cells (GFP, green) forming the subepidermal nerve plexus stained positive to p75NTR (E; red), S100 (F; red), and SOX10 (G and G'; red) glial markers.

(H–J) A subset of *Myf5*+ cells (GFP, green) expressed the non-myelinating SC marker INTEGRIN α1 (H; red; arrowhead), while other *Myf5*+ cells co-localized with myelin basic protein. (I) Some *Myf5*+ cells (GFP, green) co-localized with myelin basic protein (MBP, red), and thus constitute myelinating SCs (arrows). A subset of *Myf5*+ cells lacked co-localization with MBP, and thus constitute non-myelinating SCs (arrowhead). (J) An example of non-myelinating *Myf5*+ cells traced by TdTomato reporter (red, arrowhead). MBP staining is shown in green (arrow).

All sections were counterstained with Hoechst 33258 (blue). Scale bars represent 50 μm in (A), (C), and (D), 25 μm in (B), 20 μm in (E), (F), (G), and (J), and 10 μm in (G'), (H), and (I).

In Situ Localization of Ventral *Myf5-creSor+* Cells Corroborates Their Schwann Cell Identity

To investigate the identity and localization of *Myf5*+ cells in the dermis, we first analyzed ventral skin sections of adult *Myf5cre/+;R26TdTomato* mice. *Myf5-creSor+* cells presented a regular fiber-like pattern (Figures 2A and 2B) reminiscent of Schwann cells of the superficial cutaneous nerve network (Gresset et al., 2015). In fact, a distinct subset of *Myf5*+ cells in subepidermal location showed a unique morphology, with long processes expanding from the cell body (Figure 2B, open arrowheads). This is characteristic of terminal Schwann cells (teloglia) that ensheath nociceptive nerve endings at the dermo-epidermal inter-face (Gresset et al., 2015). To better understand the spatial distribution of *Myf5*+ cells, we performed whole-mount ventral dermis analyses (Fujiwara et al., 2011; Tschachler et al., 2004) of the *Myf5cre/+;R26EYFP* strain. *Myf5*+ cells (detected with anti-GFP) formed a subepidermal network (Figure 2C) of elongated bipolar cells that were associated with NF200+ peripheral nerves (Figure 2D). The *Myf5*+ cells also co-localized with glial markers p75NTR, S100β, and SOX10 (Figures 2E–2G'), and presented phenotypes consistent with both myelinating and non-myelinating Schwann cells. Non-myelinating Schwann cells were INTEGRIN α1+ (Figure 2H, arrowhead) and myelin basic protein negative (MBP−) (Figure 2I, arrowhead; Figure 2J).
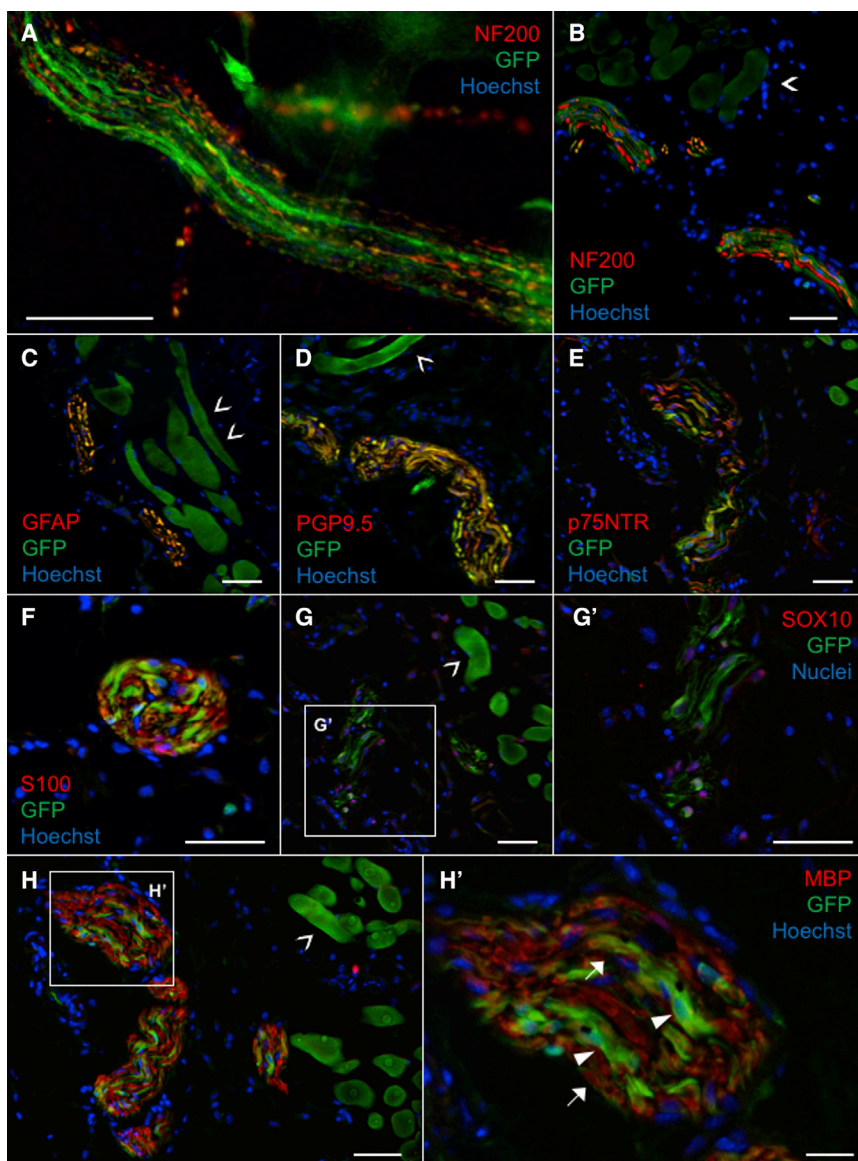
Figure 3. *Myf5* Is Expressed by Cells Ensheathing Thick Nerve Bundles at the Level of the Dermal *panniculus carnosus* Muscle

(A and B) Immunostaining of *Myf5^cre/+*; *R26^EYFP* mice dermal whole-mount (A) and ventral skin sections (B) showing thick NF200^+ (red) nerve bundles ensheathed by *Myf5^+* Schwann cells (GFP, green).

(B–H) *Panniculus camosus* muscle was traced by this construct (GFP, green; open arrowheads), as well as thick nerve bundles that co-stained with GFAP (C; red), PGP9.5 (D; red), p75NTR (E; red), S100 (F, red), and SOX10 (G and G'; red). Analysis of MBP (H and H'; red) revealed some co-localization of *Myf5^+* cells (GFP, green), indicative of myelinating (MBP^+) Schwann cells (arrows). Non-myelinating Schwann cells (arrowheads) were also clearly detected.

All sections were counterstained with Hoechst 33258 (blue). Scale bars represent 50 μm in (A), 25 μm in (B) to (H), and 20 μm in (H').

MBP^+ myelinating Schwann cells were also detected, although GFP expression was greatly diminished (Figure 2I, arrows).

At the deep dermis, thicker NF200^+ and PGP9.5^+ nerve bundles (Figures 3A, 3B, and 3D) were ensheathed by *Myf5^+* cells that co-localized with glial markers GFAP, p75NTR, S100β, and SOX10 (Figures 3C–3G'). These nerves form the subcutaneous plexus at the level of the dermal *panniculus carnosus* muscle (Naldaiz-Gastesi et al., 2016), which was also traced by *Myf5-cre^Sor* (open arrowheads in Figures 3B–3D, 3G, and 3H). Again, both myelinating (Figure 3H', arrows) and non-myelinating (Figure 3H', arrowheads) Schwann cells were detected as assessed by co-localization with MBP.

In the hair follicles, glial cells forming the mechanosensory lanceolate complex (Li and Ginty, 2014) were also *Myf5-cre^Sor+* (Figure 4A). Hair-follicle-associated *Myf5^+* cells were p75NTR^+, S100β^+, and NESTIN^+ (Figures 4B–4E), as described for the lanceolate complex glial cells (Johnston et al., 2013). In addition, *Myf5^+* cells were occasionally detected in three other locations (Figures S3–S5): (1) perivascular *Myf5^+* cells (Figure S3) were consistent with a pericyte identity, as they displayed a characteristic morphology (Figures S3C and S3D; arrows) and co-expressed pericytic markers α-smooth muscle actin (αSMA) and platelet-derived growth factor receptor β (PDGFRβ); (2) dermal nerve cells ensheathing axons in SOX2^+ touch domes (Reinisch and Tschachler, 2005) were also *Myf5^+* (Figure S4); and
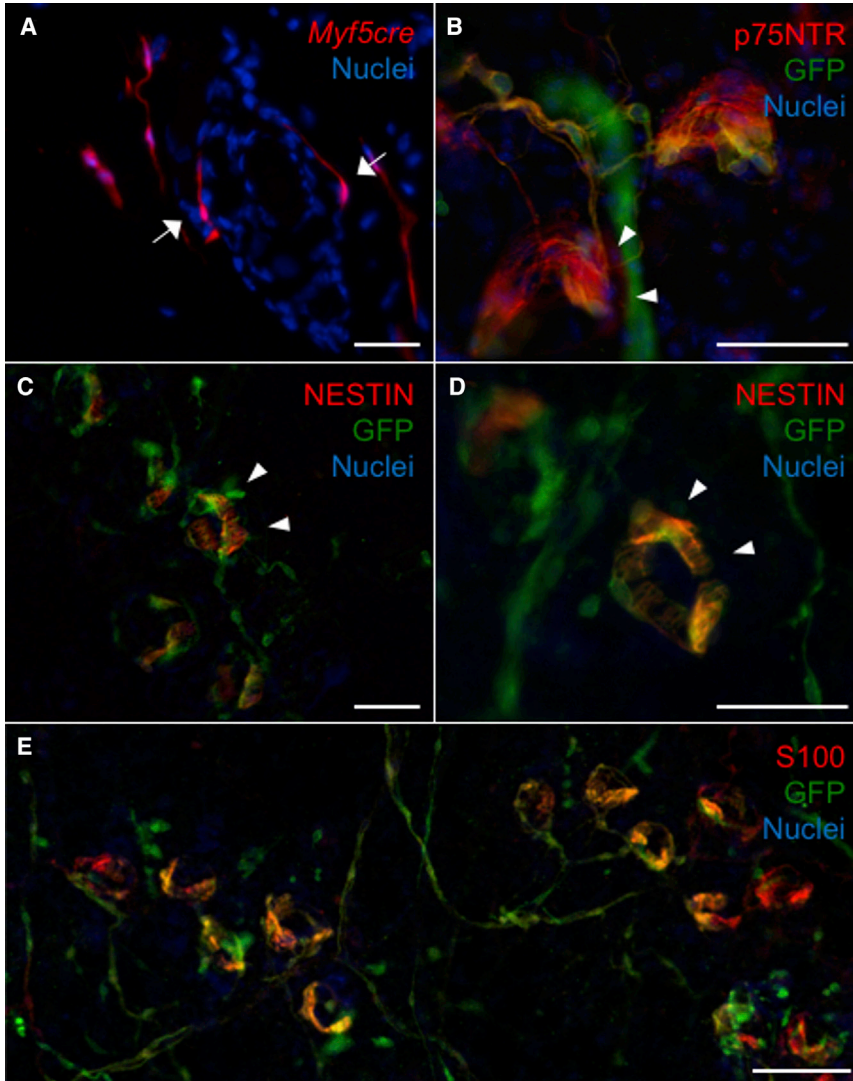
Figure 4. Schwann Cells Forming the Lanceolate Complexes of Hair Follicles Are Traced by *Myf5*^{cre/+};*R26*^{EYFP}

(A) *Myf5* expression (TdTomato, red) in sections of *Myf5*^{cre/+};*R26*^{TdTomato} was observed in lanceolate Schwann cells (SCs) surrounding hair follicles (arrows).

(B–E) Terminal SCs (GFP, green) analyzed in dermal whole-mount preparations of *Myf5*^{cre/+};*R26*^{EYFP} presented finger-shaped processes (arrowheads in B–D) and co-stained to p75NTR (B; red), NESTIN (C and D; red), and S100 (E; red).

All sections were counterstained with Hoechst 33258 (blue). Scale bars represent 25 μm in (A) to (D) and 50 μm in (E). See also Figures S3–S5.

(3) hair-follicle melanocytes were adjacent to the dermal papilla (Figure S5).

In all, these results demonstrated that the small (but reproducible) population of ventral *Myf5*⁺ cells are mainly composed of Schwann cells, and also includes rare cells of possible mesenchymal origin such as pericytes, an identity associated with dermal stem cell subsets in human skin (Etxaniz et al., 2014; Feisst et al., 2014; Ruetze et al., 2013; Yamanishi et al., 2012), as well as hair-follicle-associated melanocytes.

Sox2 Expression Levels Correlate with Neural Competence of Mouse Ventral Precursors

The neural competence of dermal precursor cells isolated from human foreskin (and mouse dorsal skin) is regulated by the expression levels of SOX2 (Etxaniz et al., 2014).

To test whether this is also the case for mouse ventral dermis, we separated dermal sphere cells from *Sox2*^{+/EGFP} mice by FACS according to their EGFP expression levels into SOX2-high, -medium, -low, and -negative populations (Figure 5). The endogenous *Sox2* mRNA levels correlated with EGFP, as determined by qRT-PCR (Figure 5B). *In vitro* differentiation of freshly isolated cell populations and immunofluorescence analyses with anti-GFAP, anti-βIII TUBULIN, and anti-GFP antibodies (surrogate for SOX2; Figures 5D–5G) demonstrated that neural competence was restricted to SOX2^{medium} and SOX2^{high} cell fractions, and correlated with the *Sox2* mRNA levels of each fraction. Morphology of the SOX2⁺ cells in the differentiated cultures was consistent with a neural identity (Figures 5E and 5G–5I). This was corroborated by co-expression in differentiated cells of markers PGP9.5,
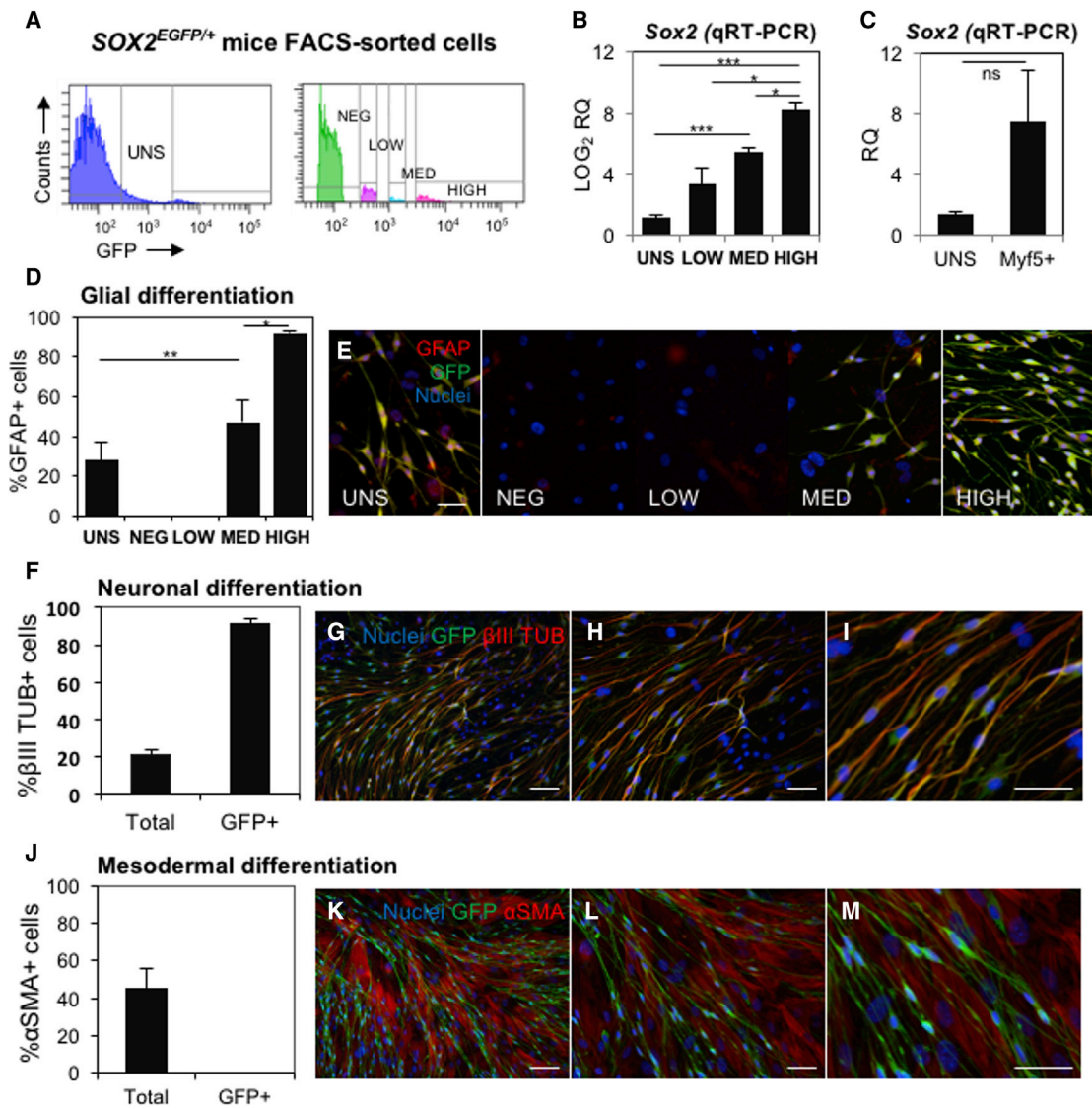
Figure 5. Neural Competence of Ventral Precursors Correlates with *Sox2* Expression Levels

(A) Ventral dermis-derived sphere cultures from *Sox2*^EGFP/+ mice were sorted by FACS into SOX2-negative (NEG), -low (LOW), -medium (MED), and -high (HIGH) subpopulations according to their EGFP levels.

(B) *Sox2* mRNA levels of separated cell fractions measured by qRT-PCR. Log$_2$ relative quantification (LOG$_2$ RQ) is shown in comparison with the NEG fraction. Mean values and SEM are represented (n = 3). Statistical significance (two-tailed unpaired t test): ***p = 0.0003 for comparison of HIGH versus UNS, *p = 0.0113 for HIGH versus LOW, *p = 0.0113 for HIGH versus MED, and ***p = 0.0003 for UNS versus MED. No statistical significance (ns) was found in all other comparisons.

(C) *Sox2* mRNA levels measured in the UNS and *Myf5*^+ cell fractions measured by qRT-PCR. The mean RQ value is represented for each fraction in comparison with the *Myf5*^− cell fraction. Error bars indicate SEM (n = 4). Statistical analysis value (two-tailed unpaired t test) was not significant (p = 0.0654).

(D) *In vitro* glial differentiation of UNS, NEG, LOW, MED, and HIGH populations isolated from *Sox2*^EGFP/+ dermal cultures. Quantification of the percentage of GFAP$^+$ cells in relation to the total number of cells. Error bars indicate SEM (n = 3). Statistical significance (two-tailed unpaired t test) values were **p = 0.0021 for comparison of UNS versus HIGH fraction and *p = 0.0149 for HIGH versus MED. No statistical significance was found in any other comparisons.

(E) Representative images of *in vitro* differentiated cultures of the UNS, NEG, LOW, MED, and HIGH cell fractions, stained with anti-GFP (Sox2^EGFP, green) and anti-GFAP (red).

(F) *In vitro* neuronal differentiation of unsorted *Sox2*^EGFP/+ dermal cultures. Quantification of the percentage of βIII TUBULIN$^+$ cells in relation to the total number of cells and GFP$^+$ cells are shown. Error bars indicate SEM (n = 3).

(legend continued on next page)

TH, p75NTR, and NESTIN (Figure S6). In contrast, SOX2+ cells showed no mesodermal differentiation capacities, as assessed by co-expression of αSMA marker (Figures 5J–5M). Finally, to analyze whether the increased neural competence of *Myf5*+ cells also correlated with *Sox2* expression, spheres from *Myf5^cre/+;R26^EYFP* mice were sorted into *Myf5*+ and *Myf5*− fractions and the *Sox2* mRNA levels were measured by qRT-PCR (Figure 5C). *Sox2* mRNA expression was 6.9-fold higher in the *Myf5*+ fraction (although non-significant). Overall, these results indicate that the neural competence of ventral dermal precursors might be regulated by SOX2 expression levels, as previously demonstrated for dorsal precursors (Etxaniz et al., 2014).

Myf5+ Cells in the Ventral Dermis Partially Overlap with Resident SOX2+ Cells

To define the relationship between SOX2+ and *Myf5*+ cells in the ventral dermis, we analyzed skin biopsies of *Sox2^+/EGFP* mice in dermal whole-mount preparations. At the subepidermal level, SOX2+ cells (stained with anti-GFP) were associated with the cutaneous peripheral nerve plexus, where they ensheathed NF200+ axons and co-stained with glial marker S100β (Figures 6A–6C). In hair follicles, SOX2 expression was localized in the lanceolate complexes (arrows in Figure 6D; Figures 6D–6F). Each receptor was individually innervated by a subset of peripheral axons that sprouted out from a dense network of NF200+ dermal nerves (Figure 6E). Lanceolate ending SOX2+ cells co-stained with NESTIN and S100β (Figures 6G–6H'). Additionally, SOX2+ cells were occasionally detected at the dermal papilla/dermal cup of some hair follicles (arrowheads; Figures 6D and 6G). SOX2+ pericytes were not detected. Since both SOX2+ and *Myf5*+ cells of ventral dermis overlap in similar dermal compartments, and to ascertain whether these markers were present in the same cells, we crossed *Myf5^cre/+;R26^TdTomato* mice with *Sox2^+/EGFP*. The analysis of whole-mount samples from the ventral dermis of *Myf5^cre/+;R26^TdTomato*; *Sox2^+/EGFP* triple transgenic mice confirmed that lanceolate ending *Myf5*+ cells (seen as TdTomato+ cells in these experiments) co-expressed SOX2 (arrows in Figures 6I and 6J). Both markers were also co-expressed by Schwann cells of the cutaneous plexus, although this was more difficult to visualize due to the apparently lower SOX2 expression levels (data not shown).

Schwann Cells in the Ventral Dermis Are Not Traced by a More Restricted *Myf5* Lineage Strain

Tracing of Schwann cells by *Myf5* expression would in principle be unexpected. Of note, a cause for concern with the *Myf5^tm3(cre)Sor* mouse model is that transgene expression is constitutive, and widespread when crossed with R26YFP (Eppig et al., 2015 and data not shown). To clarify whether tracing by the *Myf5-cre^Sor* transgene was truly indicative of *Myf5*+ cell lineage or was otherwise aberrant, we used a second *cre*-expressing strain (*B195AP-cre*) that traces a more restricted subset (17.6% in the dorsal dermis) of bona fide *Myf5*+ cells (Naldaiz-Gastesi et al., 2016). In the ventral dermis, 0.7% of sphere cells were B195AP+ (EYFP+), as assessed by flow cytometry (Figure 7A). *In vitro* glial differentiation of B195AP-positive and -negative cell fractions showed that only the cells negative for *Myf5* expression were able to generate GFAP+ cells. Furthermore, B195AP+ cells gave rise to MYH2+ myotubes *in vitro* (Figures 7B and 7C), which is consistent with tracing of *panniculus carnosus*-derived muscle satellite stem cells by this strain (Figures 7D and 7E; see also Naldaiz-Gastesi et al., 2016). Interestingly, SOX2 expression co-localized with B195AP− cells (Figures 7F and 7F'). Finally, no co-localization of B195AP+ cells was observed *in situ* with nerves and Schwann cells, as detected by absence of co-expression or vicinity with cells expressing markers PGP9.5, p75NTR, S100β, and NF200 (Figures 7G–7J). These results suggest that ventral dermal Schwann cells traced by the *Myf5-cre^Sor* transgene do not belong to the *Myf5*+ cell lineage, and are most likely explained by aberrant *cre* recombinase expression in the *Myf5-cre^Sor* mice.

DISCUSSION

In the last few years, dermal stem/precursor cells and different subsets of fibroblasts have been isolated and variously named by independent research groups. Clearly, the field is in need of harmonization and clarification. This is due in part to the developmental regionalization of the dermis and to the variety of ill-described dermal stem cell niches, but also to the lack of markers that uniquely distinguish stem cells.

In this article, we demonstrate that the neural-competent cells in ventral dermis are Schwann cells aberrantly traced by the *Myf5-cre^Sor* construct. This is certainly true for ventral dermis and seems probable for dorsal dermis

---

(G–I) Representative images of differentiated cultures, stained with anti-GFP (Sox2^EGFP, green) and anti-βIII TUBULIN (βIII, red).

(J) *In vitro* mesodermal differentiation of unsorted *Sox2^EGFP/+* dermal cultures. Quantification of the percentage of αSMA+ cells in relation to the total number of cells and GFP+ cells are shown. Error bars indicate SEM (n = 3).

(K–M) Representative images of differentiated cultures, stained with anti-GFP (Sox2^EGFP, green) and anti-αSMA (red). Nuclei were counterstained with Hoechst 33258 (blue) in all panels.

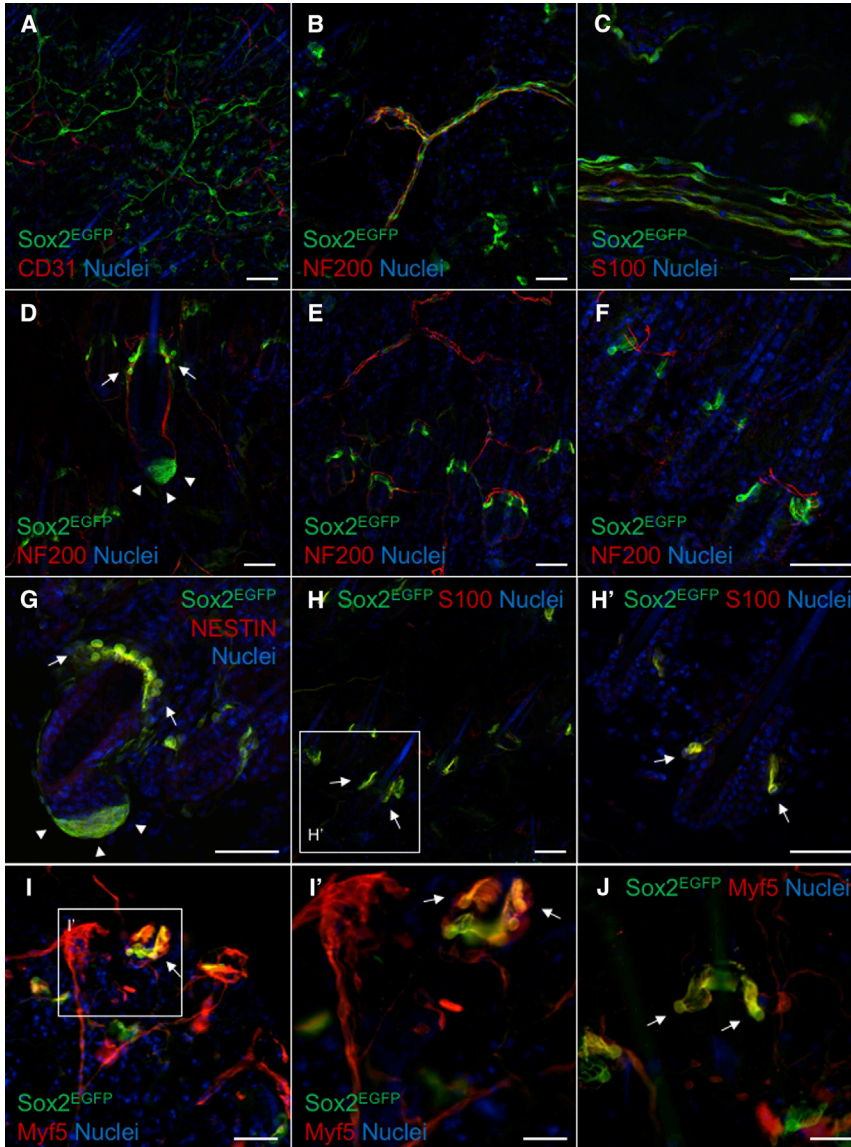Scale bars represent 25 μm in (E), (H), (I), (L), and (M), and 50 μm in (G) and (K). See also Figure S6.

Figure 6. *In Situ* Localization of Sox2^EGFP+ Cells in Mouse Ventral Dermis

(A–C) Immunostaining of ventral dermal whole-mount preparations from *Sox2^EGFP/+* mice. *Sox2^EGFP* is expressed in peripheral nerve endings innervating the skin. (A) SOX2⁺ cells (Sox2^EGFP; green) detected in the subepidermal nerve plexus, which does not co-localize with CD31⁺ blood vessels (red); and (B) ensheathing NF200⁺ nerve fibers (red). (C) Deeper in the dermis, Sox2^EGFP cells (green) forming thick nerve bundles co-expressed glial marker S100 (red).

(D) In hair follicles (HFs) *Sox2* expression (Sox2^EGFP, green) is detected in the lanceolate complexes (arrows) and in a subset of HF dermal papillae (arrowheads).

(E and F) SOX2⁺ cells (Sox2^EGFP, green) located in the bulge region of HFs innervated by NF200⁺ nerve endings (red).

(G–H') Lanceolate complex cells expressed NESTIN (G; red) and S100 (H and H'; red) (arrows). Dermal papilla/dermal cup cells are marked with arrowheads in (G).

(I–J) Dermal whole-mount preparations of *Myf5^cre/+;R26^TdTomato;Sox2^+/EGFP* showing co-expression of Myf5 (TdTomato, red) and Sox2^EGFP (green) in lanceolate complexes (arrows).

All sections were counterstained with Hoechst 33258 (blue). Scale bars represent 50 μm in (A) to (I) and 25 μm in (I') and (J).

as well, although most dorsal dermal cells are traced by *Myf5* expression, and this fact complicates the matter of discriminating among multiple components of the cell fractions. Tracing by *Myf5* expression by a second strain (*B195AP-cre*) showed that Schwann cells do not originate in a bona fide *Myf5⁺* cell lineage. Thus the tracing by *Myf5-cre^Sor* mice (Jinno et al., 2010) does not actually represent the existence of a *Myf5⁺* cell population that generates Schwann cells. A similar picture may emerge from *Dermo1* (*Twist2*)⁺ cell fate analyses (Krause et al., 2014), since the tracing construct used by these authors also presents widespread expression (including neural tissue), similar to *Myf5-cre^Sor* mice (Eppig et al., 2015).

Adult dermal stem cells of diverse niches are all considered to be SOX2⁺ (a marker that, once more, is not specific for dermal stem cells [Agabalyan et al., 2016]). In mouse dorsal skin, the diverse SOX2⁺ cell niches are well characterized (Biernaskie et al., 2009; Clavel et al., 2012; Driskell et al., 2009; Lesko et al., 2013) but the expression levels of this transcription factor are cell-context dependent and highly dynamic. Besides, Schwann cell dedifferentiation in response to wounding accounts for the majority of SOX2⁺ cells populating the wound bed (Johnston et al., 2013). In this context, we showed here that cell populations aberrantly traced by the *Myf5-cre^Sor* construct seem to be coincident with those previously described as SOX2⁺ by diverse groups. In our hands, *in situ* SOX2⁺ compartments matched between ventral and dorsal skin *of Sox2^+/EGFP* mice (data not shown).
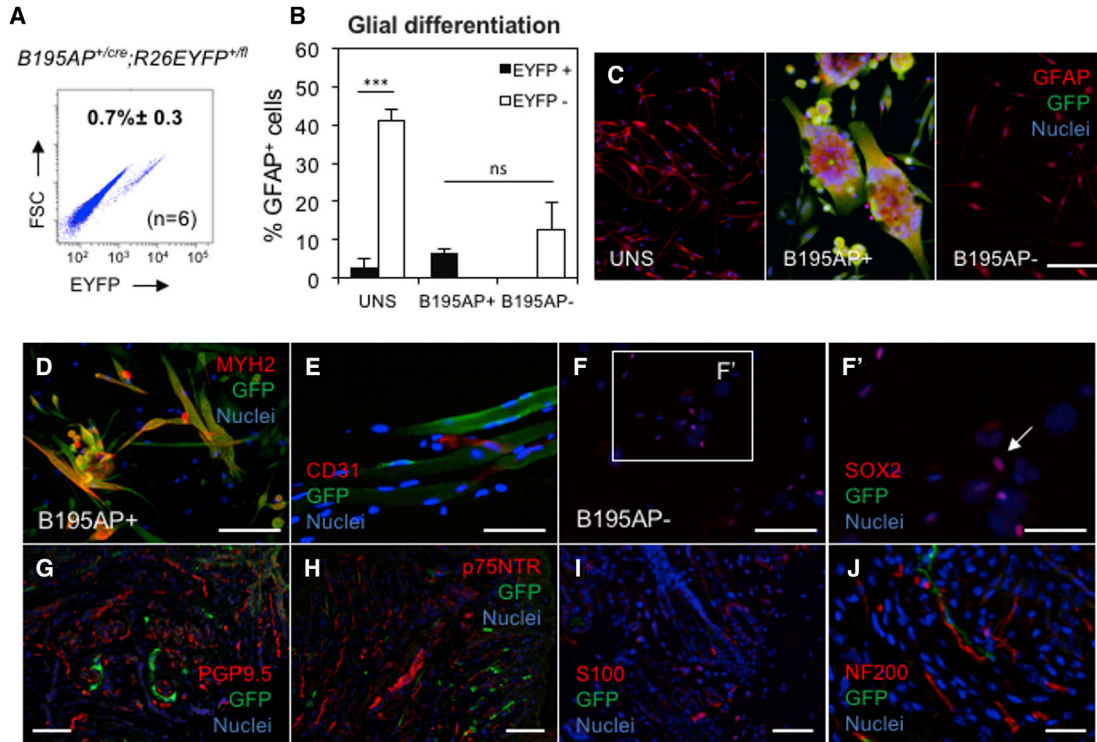
Figure 7. Neural-Competent Cells of Mouse Ventral Dermis Do Not Belong to the *Myf5*+ Lineage

(A) *B195AP*+ cell percentages (mean ± SD) were determined by flow cytometry (EYFP expression) in dermal sphere cultures from *B195AP*$^{cre/+}$;*R26*^{EYFP} mouse ventral skin (n, number of biological replicates).

(B) *In vitro* glial differentiation of unsorted (UNS) and FACS-sorted *B195AP*+ and *B195AP*− cell fractions from *B195AP*$^{cre/+}$;*R26*^{EYFP} ventral dermal spheres. Quantification of the neural progeny as percent GFAP+ cells in UNS, *B195AP*+, and *B195AP*− cell fractions is shown in relation to the total number of cells. Bars represent means ± SEM. Statistical significance values (determined by two-tailed unpaired t test) were ***p = 0.0006 for comparison of EYFP+ versus EYFP− in UNS condition and p = 0.4596 (not significant; ns) for EYFP+ (*B195AP*+) versus EYFP− (*B195AP*−) fractions.

(C–F) Representative immunofluorescence (IF) images of *in vitro* differentiated UNS, *B195AP*+, and *B195AP*− cell fractions (C) stained with anti-GFP (B195AP, green) and anti-GFAP antibody (red). *B195AP*+ cells (GFP, green) co-expressed the myogenic marker MYH2 (D; red). SOX2 was detected only in the *B195AP*− fraction (F and F′; red nuclei; arrow). (E) In ventral skin sections of *B195AP*$^{cre/+}$/*R26*^{EYFP}, muscle satellite cells were traced by *B195AP*^{cre} (GFP, green).

(G–J) *B195AP* (GFP, green) did not co-localize or ensheath nerves stained with PGP9.5 (G; red), p75NTR (H; red), S100 (I; red), and NF200 (J, red).

All IFs were counterstained with Hoechst 33258 (blue). Scale bars represent 25 μm in (E) and (F′) and 50 μm in all other panels.

In conclusion, aberrantly traced *Myf5-cre*$^{Sor+}$ Schwann cells generate neural lineages (mostly Schwann cells) upon *in vitro* differentiation in a SOX2-level-dependent manner. This report sheds light on the identification of adult ventral trunk neural precursor cells and demonstrates that they correspond to dedifferentiated peripheral glia, which derive from the neural crest (Gresset et al., 2015).

EXPERIMENTAL PROCEDURES

Animals

Mice (8- to 12-weeks-old) were used in accordance with the relevant Spanish and European guidelines after approval by the Biodonostia Animal Care Committee. Transgenic lines (described in

Table S1) were purchased from JaxMice with the exception of *Sox2*$^{+/EGFP}$ mice, which were donated by Dr. K. Hochedlinger (Harvard University) and *B195AP-cre* mice, a gift of Dr. J.J. Carvajal (Centro Andaluz de Biología del Desarrollo).

Cell Isolation, Culture, and Differentiation

Animals were euthanized by CO_2 inhalation and the dorsal and ventral skin carefully dissected. Dermal cells were processed and put in suspension culture as described by Etxaniz et al. (2014). Dermal sphere cells were separated by FACS (as detailed below), plated onto 12-mm coverslips coated with extracellular matrix (ECM) secreted from 804G cells, growth in adherence, and differentiated in Schwann medium for an additional 7–12 days as described previously (Gago et al., 2009). For neuronal differentiation, dermal spheres were disaggregated and directly plated onto

a specially designed coating on glass coverslips (Garcia-Parra et al., 2014) in Neurobasal medium supplemented with 1% L-glutamine (Sigma-Aldrich), 1% P/S (Sigma-Aldrich), 2% B27 Supplement (Gibco), 1% N2 Supplement (Gibco), 1% fetal bovine serum (ATCC), 50 ng/mL nerve growth factor β (Sigma-Aldrich), and 50 ng/mL brain-derived neurotrophic factor (Peprotech). For mesodermal differentiation, dermal spheres were disaggregated and directly plated into 12-mm diameter 804G ECM-coated coverslips in the presence of DMEM supplemented with 1% L-glutamine (Sigma-Aldrich), 1% P/S (Sigma-Aldrich), 20% fetal bovine serum (Lonza), and 10 ng/mL transforming growth factor βIII (Gibco). Cells were maintained in differentiation media for 10–14 days.

Cell Sorting

Dermal spheres at day 7 of proliferation were dissociated to a single-cell suspension with 0.25% trypsin-EDTA solution (Sigma-Aldrich), resuspended in sorting buffer, and analyzed in a FACSAria III (Becton Dickinson) with TOPRO exclusion of viable populations. Cell fractions from $Myf5^{cre/+}$;$R26EYFP$ mice were sorted as EYFP-positive and -negative, and $SOX2^{+/EGFP}$ samples were separated according to their SOX2 expression levels. Cells were collected for expansion as described by Etxaniz et al. (2014).

RNA Extraction and Real-Time qPCR

Total RNA was extracted from sorted cells using an miRNeasy micro kit with the automatic QIAcube workstation (Qiagen). Reverse transcription was performed using RNA to cDNA High Capacity Kit (Applied Biosystems). The cDNA of selected genes (SOX2 expression analysis) was specifically amplified (14 cycles) using a PreAmp Master Mix Kit (Applied Biosystems). TaqMan probe and SYBR green-based gene expression analyses were performed using 96- and 384-well plates on 7900HT (Applied Biosystems) and Light Cycler 96 (Roche) real-time PCR systems, respectively. Relative quantification analyses were carried out by using the RQ ($2^{-\Delta\Delta Ct}$) method (Livak and Schmittgen, 2001). The significance threshold was set at a fold change of 2. TaqMan probes and SYBR green primer sequences are listed in Tables S2 and S3, respectively.

Immunofluorescence on Coverslips, Frozen Skin Sections, and Dermal Whole Mounts

Dermal sphere cultures and *in vitro* differentiated cells were fixed, permeabilized, stained, and imaged as described by Etxaniz et al. (2014). Tissue samples were embedded in Tissue-Tek (OCT compound, Sakura) and 5 μm-thick cryostat sections were cut. The staining was performed as described by Jinno et al. (2010). Antibodies used are detailed in Table S4. Dermal whole-mount immunofluorescence has been described elsewhere (Fujiwara et al., 2011; Tschachler et al., 2004).

Image Acquisition

Images were acquired on an LSM510 META confocal microscope (Zeiss) using the ZEN 2008 sp2 software package (v. 4.2), in addition to an Eclipse 80i fluorescence microscope (Nikon) using NIS elements-AR software packages (v.3.2).

Statistical Analyses

Statistical analysis was carried out using GraphPad Prism software v5.01. For multiple group comparisons, a two-tailed unpaired t test was performed. The number of biological replicates (n) for each experiment and average ± SEM are indicated when applicable, and statistical significance is indicated by *p < 0.05, **p < 0.01, and ***p < 0.001.

SUPPLEMENTAL INFORMATION

Supplemental Information includes six figures and four tables and can be found with this article online at https://doi.org/10.1016/j.stemcr.2017.09.010.

AUTHOR CONTRIBUTIONS

H.I. performed most of the experimental work. V.P.-L. helped in cell culturing, mouse genotyping, and histological characterization. U.E. performed some of the initial cell culture and differentiation experiments. A.G.-R. was responsible for mouse colony handling and co-directed experimental work. A.I. directed and financed the project. H.I. and A.I. wrote the manuscript, which was approved by all authors prior to submission.

ACKNOWLEDGMENTS

REFERENCES

Agabalyan, N.A., Hagner, A., Rahmani, W., and Biernaskie, J. (2016). SOX2 in the skin. In Sox2—Biology and Role in Development and Disease, H. Kondoh and R. Lovell-Badge, eds. (Academic Press), pp. 281–300.

Agabalyan, N.A., Rosin, N.L., Rahmani, W., and Biernaskie, J. (2017). Hair follicle dermal stem cells and skin-derived precursor cells: exciting tools for endogenous and exogenous therapies. Exp. Dermatol. 26, 505–509.

Biernaskie, J., Paris, M., Morozova, O., Fagan, B.M., Marra, M., Pevny, L., and Miller, F.D. (2009). SKPs derive from hair follicle precursors and exhibit properties of adult dermal stem cells. Cell Stem Cell 5, 610–623.

Christ, B., Huang, R., and Scaal, M. (2007). Amniote somite derivatives. Dev. Dyn. 236, 2382–2396.

Clavel, C., Grisanti, L., Zemla, R., Rezza, A., Barros, R., Sennett, R., Mazloom, A.R., Chung, C.-Y., Cai, X., Cai, C.-L., et al. (2012). Sox2 in the dermal papilla niche controls hair growth by fine-tuning BMP signaling in differentiating hair shaft progenitors. Dev. Cell *23*, 981–994.

Driskell, R.R., Giangreco, A., Jensen, K.B., Mulder, K.W., and Watt, F.M. (2009). Sox2-positive dermal papilla cells specify hair follicle type in mammalian epidermis. Development *136*, 2815–2823.

Dupin, E., and Sommer, L. (2012). Neural crest progenitors and stem cells: from early development to adulthood. Dev. Biol. *366*, 83–95.

Eppig, J.T., Blake, J.A., Bult, C.J., Kadin, J.A., and Richardson, J.E. (2015). The Mouse Genome Database (MGD): facilitating mouse as a model for human biology and disease. Nucleic Acids Res. *43*, D726–D736.

Etxaniz, U., Pérez-San Vicente, A., Gago-López, N., García-Dominguez, M., Iribar, H., Aduriz, A., Pérez-López, V., Burgoa, I., Irizar, H., Muñoz-Culla, M., et al. (2014). Neural-competent cells of adult human dermis belong to the Schwann lineage. Stem Cell Reports *3*, 774–788.

Feisst, V., Brooks, A.E., Chen, C.J., and Dunbar, P.R. (2014). Characterization of mesenchymal progenitor cell populations directly derived from human dermis. Stem Cells Dev. *23*, 631–642.

Fernandes, K.J.L., McKenzie, I.A., Mill, P., Smith, K.M., Akhavan, M., Barnabé-Heider, F., Biernaskie, J., Junek, A., Kobayashi, N.R., Toma, J.G., et al. (2004). A dermal niche for multipotent adult skin-derived precursor cells. Nat. Cell Biol. *6*, 1082–1093.

Fujiwara, H., Ferreira, M., Donati, G., Marciano, D.K., Linton, J.M., Sato, Y., Hartner, A., Sekiguchi, K., Reichardt, L.F., and Watt, F.M. (2011). The basement membrane of hair follicle stem cells is a muscle cell niche. Cell *144*, 577–589.

Gago, N., Pérez-López, V., Sanz-Jaka, J.P., Cormenzana, P., Eizaguirre, I., Bernad, A., and Izeta, A. (2009). Age-dependent depletion of human skin-derived progenitor cells. Stem Cells *27*, 1164–1172.

Garcia-Parra, P., Naldaiz-Gastesi, N., Maroto, M., Padin, J.F., Goicoechea, M., Aiastui, A., Fernandez-Morales, J.C., Garcia-Belda, P., Lacalle, J., Alava, J.I., et al. (2014). Murine muscle engineered from dermal precursors: an in vitro model for skeletal muscle generation, degeneration, and fatty infiltration. Tissue Eng. Part C Methods *20*, 28–41.

Gresset, A., Coulpier, F., Gerschenfeld, G., Jourdon, A., Matesic, G., Richard, L., Vallat, J.-M., Charnay, P., and Topilko, P. (2015). Boundary caps give rise to neurogenic stem cells and terminal glia in the skin. Stem Cell Reports *5*, 278–290.

Hunt, D.P., Jahoda, C., and Chandran, S. (2009). Multipotent skin-derived precursors: from biology to clinical translation. Curr. Opin. Biotechnol. *20*, 522–530.

Jessen, K.n.R., Mirsky, R., and Lloyd, A.C. (2015). Schwann cells: development and role in nerve repair. Cold Spring Harb. Perspect. Biol. *7*, a020487.

Jinno, H., Morozova, O., Jones, K.L., Biernaskie, J.A., Paris, M., Hosokawa, R., Rudnicki, M.A., Chai, Y., Rossi, F., Marra, M.A., et al. (2010). Convergent genesis of an adult neural crest-like dermal stem cell from distinct developmental origins. Stem Cells *28*, 2027–2040.

Joannides, A., Gaughwin, P., Schwiening, C., Majed, H., Sterling, J., Compston, A., and Chandran, S. (2004). Efficient generation of neural precursors from adult human skin: astrocytes promote neurogenesis from skin-derived stem cells. Lancet *364*, 172–178.

Johnston, A.P.W., Naska, S., Jones, K., Jinno, H., Kaplan, D.R., and Miller, F.D. (2013). Sox2-mediated regulation of adult neural crest precursors and skin repair. Stem Cell Reports *1*, 38–45.

Krause, M.P., Dworski, S., Feinberg, K., Jones, K., Johnston, A.P.W., Paul, S., Paris, M., Peles, E., Bagli, D., Forrest, C.R., et al. (2014). Direct genesis of functional rodent and human schwann cells from skin mesenchymal precursors. Stem Cell Reports *3*, 85–100.

Lesko, M.H., Driskell, R.R., Kretzschmar, K., Goldie, S.J., and Watt, F.M. (2013). Sox2 modulates the function of two distinct cell lineages in mouse skin. Dev. Biol. *382*, 15–26.

Li, L., and Ginty, D.D. (2014). The structure and organization of lanceolate mechanosensory complexes at mouse hair follicles. Elife *3*, e01901.

Livak, K.J., and Schmittgen, T.D. (2001). Analysis of relative gene expression data using real-time quantitative PCR and the $2^{-\Delta\Delta C}$T method. Methods *25*, 402–408.

Millar, S.E. (2005). An ideal society? Neighbors of diverse origins interact to create and maintain complex mini-organs in the skin. PLoS Biol. *3*, e372.

Naldaiz-Gastesi, N., Goicoechea, M., Alonso-Martín, S., Aiastui, A., López-Mayorga, M., García-Belda, P., Lacalle, J., San José, C., Araúzo-Bravo, M.J., Trouilh, L., et al. (2016). Identification and characterization of the dermal panniculus carnosus muscle stem cells. Stem Cell Reports *7*, 411–424.

Ohtola, J., Myers, J., Akhtar-Zaidi, B., Zuzindlak, D., Sandesara, P., Yeh, K., Mackem, S., and Atit, R. (2008). beta-Catenin has sequential roles in the survival and specification of ventral dermis. Development *135*, 2321–2329.

Olivera-Martinez, I., Viallet, J.P., Michon, F., Pearton, D.J., and Dhouailly, D. (2004). The different steps of skin formation in vertebrates. Int. J. Dev. Biol. *48*, 107–115.

Reinisch, C.M., and Tschachler, E. (2005). The touch dome in human skin is supplied by different types of nerve fibers. Ann. Neurol. *58*, 88–95.

Ruetze, M., Knauer, T., Gallinat, S., Wenck, H., Achterberg, V., Maerz, A., Deppert, W., and Knott, A. (2013). A novel niche for skin derived precursors in non-follicular skin. J. Dermatol. Sci. *69*, 132–139.

Tschachler, E., Reinisch, C.M., Mayer, C., Paiha, K., Lassmann, H., and Weninger, W. (2004). Sheet preparations expose the dermal nerve plexus of human skin and render the dermal nerve end organ accessible to extensive analysis. J. Invest. Dermatol. *122*, 177–182.

Yamanishi, H., Fujiwara, S., and Soma, T. (2012). Perivascular localization of dermal stem cells in human scalp. Exp. Dermatol. *21*, 78–80.